RSC Advances

RSC Publishing

COMMUNICATION

View Article Online
View Journal | View Issue

Cite this: *RSC Advances*, 2013, **3**, 6817

Received 23rd January 2013,
Accepted 19th March 2013

DOI: 10.1039/c3ra40359a

www.rsc.org/advances

Surface-decorated ZnO nanoparticles and ZnO nanocoating on electrospun polymeric nanofibers by atomic layer deposition for flexible photocatalytic nanofibrous membranes†

Fatma Kayaci, Cagla Ozgit-Akgun, Necmi Biyikli* and Tamer Uyar*

Electrospun polymeric nanofibers were either surface-decorated with zinc oxide (ZnO) nanoparticles or coated with a continuous ZnO thin film with a precise thickness (~27 nm) *via* atomic layer deposition (ALD) for the fabrication of flexible photocatalytic nanofibrous membranes.

Water pollution is a growing environmental issue which severely threatens human health. Consequently, development of novel materials for water purification and waste treatment is an important research topic.[1,2] Functional nanomaterials[3] exhibiting photocatalytic properties, along with a very high surface area, have been widely investigated, since these nanostructures are quite effective in the degradation of organic contaminants under UV light and sunlight. For instance, metal oxides such as ZnO[4] and TiO_2[5] are very well known for their photocatalytic activity and therefore, these materials in the form of nanoparticles,[4b,5a] nanorods[4c,d,5c] and nanofibers[4b,5d] have been studied intensely for water purification purposes. However, the brittle nature of these metal oxides often causes problems when they are used as a membrane. Therefore, designing photocatalytic membranes with flexible character is highly desired. For instance, flexible membranes composed of electrospun polymeric nanofibers functionalized with ZnO nanorods,[4c,d] formed by using a hydrothermal method have been shown to be effective for the photocatalytic degradation of organic molecules, so they have the potential for water purification and organic waste treatment. However, novel materials are always needed for the development of advanced filtering systems for water treatment.

In this work, polymeric nanofibers surface-decorated with ZnO nanoparticles (NPs) and a ZnO nanocoating were fabricated using a two-step approach: electrospinning and atomic layer deposition (ALD) (Fig. 1 and Fig. S1, ESI†). Initially, polymeric (nylon 6,6) nanofibers with an average fiber diameter of ~80 nm were produced *via* electrospinning technique. In the next step, ZnO was grown onto smooth surfaces of polymeric nanofibers *via* ALD[6] by altering the deposition parameters. Altering the ALD parameters resulted in various ZnO morphologies on the polymeric nanofibers; surface-decorated ZnO NPs and highly dense ZnO NPs, and a continuous ZnO nanocoating with a uniform thickness (~27 nm). The resulting ZnO nanostructures onto nanofibers are illustrated schematically in Fig. 1. The scanning electron microscopy (SEM) images clearly elucidated that the ALD process did not destroy the fibrous structure of the polymer. In addition, when compared to the pristine polymeric nanofiber, nylon–ZnO nanofibers had rougher surfaces due to the deposition of ZnO NPs and the nanocoating (Fig. 2 and Fig. S2, ESI†). Overall, the sample decorated with highly dense ZnO NPs exhibited the highest surface roughness due to the presence of a greater number of individual ZnO NPs (Fig. 2c and 3b).

The transmission electron microscopy (TEM) images clearly revealed the morphologies of ZnO deposited on polymeric nanofibers (Fig. 3 and Fig. S3, ESI†). For the sample shown in

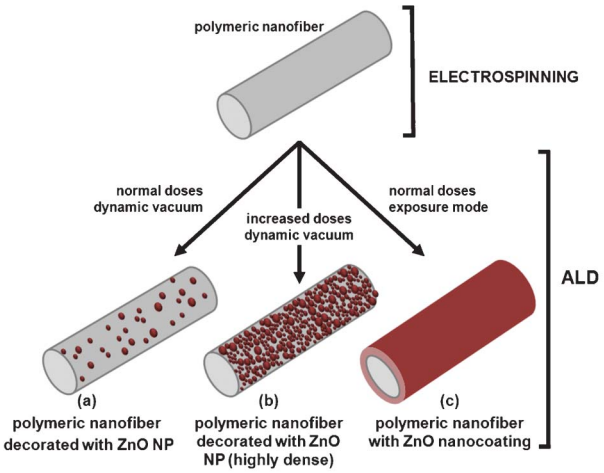

Fig. 1 Schematic representation of the formation of polymer–ZnO nanofibers: electrospinning of the polymeric nanofiber and ZnO deposition with different morphologies on the electrospun nanofiber by using various ALD parameters.

UNAM-Institute of Materials Science & Nanotechnology, Bilkent University, Ankara, 06800, Turkey. E-mail: tamer@unam.bilkent.edu.tr; biyikli@unam.bilkent.edu.tr; Fax: +90(312)266 4365; Tel: +90(312)290 3571

† Electronic supplementary information (ESI) available. See DOI: 10.1039/c3ra40359a

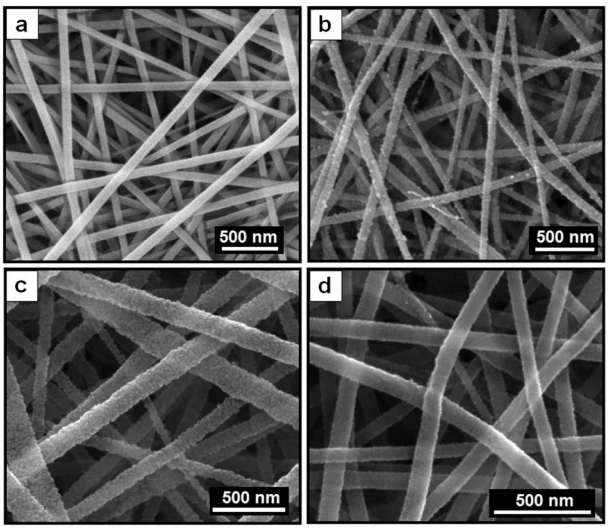

Fig. 2 SEM images of nanofibers: (a) pristine nylon, (b) nylon–ZnO NPs, (c) nylon–ZnO NPs (highly dense), and (d) nylon–ZnO nanocoating.

Fig. 3a, ALD was performed under dynamic vacuum conditions with 0.015 s pulses and 10 s purges. The resulting morphology was in the form of randomly distributed individual ZnO NPs with an average size of 20 $\pm$ 15 nm. When run for 800 cycles, this recipe resulted in a $\sim$90 nm thick uniform ZnO coating on the electrospun nylon nanofibers.[7] The deposition of highly dense ZnO NPs was obtained when the pulse times of diethylzinc (DEZn) and H_2O were both increased to 0.09 s (Fig. 3b). The TEM image shown in Fig. 3c belongs to a sample which was prepared by using the exposure mode (a trademark of Cambridge Nanotech Inc.), with 0.015 s pulses, 10 s exposures, and 10 s purges. The exposure mode keeps the precursor molecules inside the reaction chamber for a certain period of time by switching the dynamic vacuum to a static vacuum just before the precursor pulses. After the exposure, the static vacuum is switched back to a dynamic vacuum for purging. The resulting morphology was a $\sim$27 nm thick ZnO coating around the polymeric nanofibers. This process, therefore, yielded a ZnO nanocoating with a uniform thickness over the relatively large surface area of electrospun nanofibers.

All three samples were decorated with ZnO NPs or coated with a uniform ZnO thin film. The formation of NPs instead of a continuous film for the samples prepared under the dynamic vacuum conditions is not due to the limitation of diffusion, since we observed that the precursor molecules can reach every part of the nanofibrous membranes and produce either randomly distributed NPs or a continuous thin film. As the number of precursor molecules increases, the probability for these molecules to coincide with one of the reactive sites on the substrate also increases. Therefore, the increased number of ZnO NPs with the increased DEZn and H_2O doses was an expected outcome. Our results indicate that the nucleation and growth of ZnO on polymeric nanofibers proceeds through the formation of islands and subsequent coalescence of these islands to form a continuous film, *i.e.* Volmer–Weber (3D) growth. The ALD technique has been used to produce conformal and very thin inorganic coatings onto polymeric fibrous materials.[7,8] In contrast, ZnO NPs have been grown on single-walled carbon nanotubes by ALD.[9] In another study, Libera *et al.*[10] reported that the ALD of ZnO on amorphous silica forms NPs in the early stages of growth, instead of a uniform thin coating. In our study, by taking advantage of the slow nucleation and/or growth kinetics of ZnO, ZnO NPs were decorated onto polymeric nanofibers under the dynamic vacuum conditions. Although it has been shown that the number of particles can be increased by increasing the precursor doses, the parameters controlling the size of these NPs are currently unknown. Research is underway to investigate the very initial stages of growth, as well as to fully control the morphology of the resulting NPs.

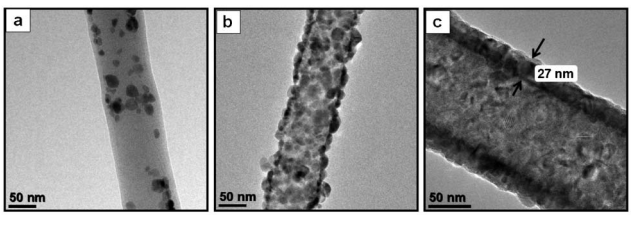

Fig. 3 Representative TEM images of nanofibers: (a) nylon–ZnO NPs, (b) nylon–ZnO NPs (highly dense), and (c) nylon–ZnO nanocoating.

The polycrystalline nature of the deposited ZnO was revealed from the selected area electron diffraction (SAED) patterns of the nylon–ZnO nanofibers (Fig. S4, ESI†), which correlate well with the X-ray diffraction (XRD) results (Fig. S5, ESI†). Moreover, bright spots on the polycrystalline diffraction rings were observed for all of the three samples, which showed the existence of large crystal grains. The intensities of the SAED patterns were different for the different morphologies due to the relative amounts of ZnO present on the nanofibers. The semi-crystalline nature of the pristine nylon nanofibers was confirmed by XRD, with two distinct diffraction peaks at 20.4° (100) and 23.0° (010, 110).[11] These peaks, although suppressed due to the deposition of ZnO, were also observed in the XRD patterns of the nylon–ZnO samples, suggesting that the crystalline structure of the polymer was not affected during the ALD process. The crystal structure of ZnO deposited onto the nanofibers by ALD was determined as hexagonal wurtzite structure from the XRD patterns of the samples, in which the diffraction peaks were indexed according to The International Centre for Diffraction Data (ICDD) (Reference Code: 01-074-0040). Similar to the SAED patterns, the intensities of the ZnO diffraction peaks in the XRD patterns were amplified as the relative amount of ZnO on the sample increased.

The surface chemical composition of the nylon–ZnO nanofibers was investigated by using X-ray photoelectron spectroscopy (XPS) (Table S1, ESI†). As expected, the C 1s, O 1s, and N 1s peaks from the polymer (nylon 6,6) were observed in the XPS scans of both of the nylon–ZnO NP samples. In the case of the nylon–ZnO nanocoating, the N 1s peak could not be detected due to the continuous layer of ZnO, as also proven by TEM analysis (Fig. 3c). In addition, contamination could increase the amount of C observed in the scans for all of the samples. The presence of a Zn $2p^3$ peaks and the increased intensity of the O 1s peaks in the XPS

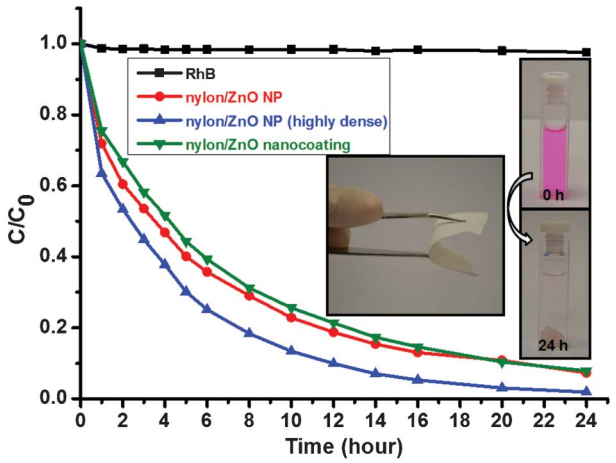

Fig. 4 The rate (C/C_0) of Rh-B degradation with and without nylon–ZnO nanofibers, by exposing UV light with a 365 nm wavelength; representative photographs of the flexible nylon–ZnO NPs (highly dense) nanofibrous membrane, and the change of color of the Rh-B solution using this membrane as a function of the UV irradiation time.

scans were assigned to the ZnO structures on the nanofibers (Table S1, ESI†). A high resolution XPS scan was also taken to confirm the formation of ZnO on the surface of the nylon nanofibers. A Zn 2p doublet, consisting of Zn $2p^{3/2}$ and Zn $2p^{1/2}$ subpeaks located at 1022.88 and 1045.86 eV respectively, was observed confirming the Zn–O bonding state (Fig. S6, ESI†).[12]

The compositional wt% of the samples was calculated from the thermogravimetric analysis (TGA) thermograms (Fig. S7, ESI†). Compositions of 17, 54, and 82 wt% ZnO were determined in the nylon–ZnO NPs, nylon–ZnO NPs (highly dense), and nylon–ZnO nanocoating samples, respectively. It was also observed that the main decomposition temperature of nylon for the nylon–ZnO samples was lower (~280 °C) compared to that of the pristine nylon nanofibers, which is ~350 °C. The lower degradation temperature observed for the nylon–ZnO nanofibers was possibly due to the catalytic activity of ZnO, resulting in earlier polymer decomposition.[7,13]

The resulting nylon–ZnO nanofibrous membranes were easily handled and folded as a free standing material due to the flexible polymeric component (Fig. 4 and Fig. S8, ESI†). In order to investigate the effect of the ZnO morphology on the efficiency of the photocatalytic activity, nylon–ZnO nanofibers with three different ZnO morphologies were tested. The photocatalytic activities of these flexible nylon–ZnO nanofibrous membranes were tested by following the photocatalytic decomposition of a model azo-reactive dye, rhodamine-B (Rh-B), under the irradiation of UV light. The changes in the absorption peaks of Rh-B at 554 nm as a function of the UV irradiation time are shown in Fig. S9, ESI.† The degradation rates of Rh-B were calculated by using the absorption peak points and defined as C/C_0 where C_0 and C represent the initial concentration of Rh-B before UV irradiation and after a specific time of UV irradiation, respectively (Fig. 4). No significant direct photolysis was observed for the blank Rh-B solution, and therefore the pink color of the dye solution did not change after UV irradiation over a period of 24 h (Fig. S9, ESI†). In contrast, the effective photocatalytic degradation of Rh-B was clearly observed for all of the Rh-B solutions containing nylon–ZnO nanofiber samples. The absorbencies of these solutions were reduced distinctly with respect to UV irradiation owing to the photocatalytic activity of the ZnO nanostructures on the nanofibers (Fig. 4 and Fig. S9, ESI†). The Rh-B solutions containing nylon–ZnO nanofiber membranes were decolorized during the UV irradiation, and the pink color of the solution almost disappeared after 24 h, revealing the successful photocatalytic decomposition of Rh-B by the nylon–ZnO nanofibers (Fig. 4 and Fig. S9, ESI†). For the nylon–ZnO NPs, 53% of the Rh-B decomposed in 4 h, and 93% decomposed in 24 h. A similar result was obtained for the nylon–ZnO nanocoating; 49% of Rh-B decomposed in 4 h and 94% decomposed in 24 h. In the case of the nylon–ZnO NP (highly dense) sample, the decomposition of Rh-B was 63% and 99% in 4 and 24 h, respectively. Therefore, the highest photocatalytic degradation rate of Rh-B was observed for the nylon–ZnO NP (highly dense) sample, which is possibly because of the presence of a large number of individual ZnO NPs, resulting in a higher surface area. This result clearly indicates that there is no need for a continuous ZnO nanocoating on the polymeric nanofibers, since surface-decorated ZnO NPs, depending on their concentration, exhibited similar or improved efficiency for the photocatalytic decomposition of model organic dye compared with the ZnO nanocoating.

In summary, we have fabricated flexible photocatalytic nanofibrous membranes by combining the electrospinning and ALD techniques. By altering the ALD parameters, various ZnO morphologies on polymeric nanofibers such as ZnO NPs or a continuous ZnO nanocoating were obtained. The nanofibrous membrane surface-decorated with highly dense ZnO NPs exhibited the highest efficiency for the photocatalytic decomposition of Rh-B dye due to its large surface area. These functional nanofibrous membranes may find applications as filtering materials for water purification and organic waste treatment. We showed that ALD can provide not only uniform and conformal coatings with precise thickness control, but can also be used to surface-decorate polymeric nanofiber templates with inorganic NPs, and the distribution density of the NPs can easily be adjusted by altering the deposition parameters. This approach can be used to produce functional flexible nanofibrous membranes for filtration, catalysis, sensors, photonics, electronics, energy and biotechnology, depending on the selection of the polymer and inorganic components.

Acknowledgements

DPT is acknowledged for the support of UNAM. T. Uyar and N. Biyikli acknowledge Marie Curie IRG for funding the NANOWEB and NEMSmart projects, respectively. F. Kayaci and C. Ozgit-Akgun acknowledge TUBITAK for the PhD Scholarship. M. Guler is acknowledged for the TEM imaging.

References

1 Q. Li, S. Mahendra, D. Y. Lyon, L. Brunet, M. V. Liga, D. Li and P. J. J. Alvarez, *Water Res.*, 2008, **42**, 4591.

2 F. Meng, S. R. Chae, A. Drews, M. Kraume, H. S. Shin and F. Yang, *Water Res.*, 2009, **43**, 1489.
3 M. M. Khin, A. S. Nair, V. J. Babu, R. Murugan and S. Ramakrishna, *Energy Environ. Sci.*, 2012, **5**, 8075.
4 (*a*) K. T. Johnson, T. E. Gribb, E. M. Smoak and I. A. Banerjee, *Chem. Commun.*, 2010, **46**, 1757; (*b*) H. Liu, J. Yang, J. Liang, Y. Huang and C. Tang, *J. Am. Ceram. Soc.*, 2008, **91**, 1287; (*c*) A. Sugunan, V. K. Guduru, A. Uheida, M. S. Toprak and M. R. Muhammed, *J. Am. Ceram. Soc.*, 2010, **93**, 3740; (*d*) Z. Chang, *Chem. Commun.*, 2011, **47**, 4427.
5 (*a*) H. Tada, T. Kiyonaga and S.-I. Naya, *Chem. Soc. Rev.*, 2009, **38**, 1849; (*b*) T. Ochiai and A. Fujishima, *J. Photochem. Photobiol., C*, 2012, **13**, 247; (*c*) M. Shang, W. Wang, W. Yin, J. Ren, S. Sun and L. Zhang, *Chem.–Eur. J.*, 2010, **16**, 11412; (*d*) T. Zhao, Z. Liu, K. Nakata, S. Nishimoto, T. Murakami, Y. Zhao, L. Jiang and A. Fujishima, *J. Mater. Chem.*, 2010, **20**, 5095.
6 (*a*) S. M. George, *Chem. Rev.*, 2010, **110**, 111; (*b*) C. Detavernier, J. Dendooven, S. P. Sree, K.F. Ludwig and J. A. Martens, *Chem. Soc. Rev.*, 2011, **40**, 5242.
7 F. Kayaci, C. Ozgit, I. Donmez, N. Biyikli and T. Uyar, *ACS Appl. Mater. Interfaces*, 2012, **4**, 6185.
8 (*a*) J. S. Jur, W. J. Sweet III, C. J. Oldham and G. N. Parsons, *Adv. Funct. Mater.*, 2011, **21**, 1993; (*b*) M. Kemell, V. Pore, M. Ritala, M. Leskelä and M. Lindén, *J. Am. Chem. Soc.*, 2005, **127**, 14178; (*c*) J. T. Korhonen, P. Hiekkataipale, J. Malm, M. Karppinen, O. Ikkala and R. H. A. Ras, *ACS Nano*, 2011, **5**, 1967.
9 (*a*) Y. S. Min, E. J. Bae, J. B. Park, U. J. Kim, W. Park, J. Song, C. S. Hwang and N. Park, *Appl. Phys. Lett.*, 2007, **90**, 263104; (*b*) Y. S. Min, I. H. Lee, Y. H. Lee and C. S. Hwang, *CrystEngComm*, 2011, **13**, 3451.
10 J. Libera, J. Elam and M. Pellin, *Thin Solid Films*, 2008, **516**, 6158.
11 J. Li, Y. Zuo, X. Cheng, W. Yang, H. Wang and Y. Li, *J. Mater. Sci.: Mater. Med.*, 2009, **20**, 1031.
12 K.-Y. Pan, Y.-H. Lin and P.-S. Lee, *J. Nanomater.*, 2011, **2012**, 279245.
13 W. Li, H. Li and Y. M. Zhang, *J. Mater. Sci.*, 2009, **44**, 2977.

